Modeling mechanophore activation within a viscous rubbery network

CrossMark

Meredith N. Silberstein [a,*], Lee D. Cremar [b], Brett A. Beiermann [c],
Sharlotte B. Kramer [a,c], Todd J. Martinez [b], Scott R. White [a,d], Nancy R. Sottos [a,c]

[a] Beckman Institute, University of Illinois at Urbana-Champaign, Urbana, IL 61801, USA
[b] Department of Chemistry, Stanford University, Stanford, CA 94305, USA
[c] Department of Materials Science and Engineering, University of Illinois at Urbana-Champaign, Urbana, IL 61801, USA
[d] Department of Aerospace Engineering, University of Illinois at Urbana-Champaign, Urbana, IL 61801, USA

ARTICLE INFO

ABSTRACT

Mechanically induced chemical reactivity is a promising means for designing self-sensing and autonomous materials. Force sensitive chemical groups called mechanophores can be covalently linked into polymers in order to trigger specific chemical reactions upon mechanical loading. A model framework is developed to describe the response of these mechanophores to mechanical loading within an elastomeric matrix. A multiscale modeling scheme is used to couple mechanophore kinetics with rubbery elasticity. In particular, transition state theory for the population of mechanophores is modified to account for the stress-induced changes in kinetics within the solid state. The model is specified to the case of spiropyran covalently linked into a polymethacrylate (PMA) backbone. This optically trackable mechanophore (optically active through absorption and fluorescence when triggered) allows the model to be assessed in comparison to observed experimental behavior. The activation predicted by the ideal viscous elastomer model is reasonable, but consistently occurs at a larger strain than in the experiments. The glassy portion of the PMA response accounts for part of the difference in the onset of activation between experiments and the ideal elastomer model. The glassy stress response is therefore included as an additional empirically determined driving force for activation in the model. The remainder of the discrepancy between the experimental and simulation results is attributed to force inhomogeneity within the rubbery network, highlighting that the mechanophore response is correlated with local force history rather than with macroscopic stress.

© 2013 Elsevier Ltd. All rights reserved.

1. Background

   Mechanically sensitive molecular units called mechanophores can be covalently linked into polymers in order to trigger specific chemical reactions upon mechanical loading. Mechanophores present a novel means for designing multifunctional and smart materials. Efficient transmission of stress on the macroscale to force on the molecular scale results in mechanophore reactions. Mechanophores have been incorporated in a range of polymer matrices and activated under different modes of macroscopic deformation (e.g. Hickenboth et al., 2007; Caruso et al., 2009; Davis et al., 2009; Lee et al., 2010; Black et al., 2011; Beiermann et al., 2011; Kingsbury et al., 2011). In particular, the rate dependent behavior of spiropyran within linear polymethacrylate (PMA) has

---

* Corresponding author. Tel.: +1 607 255 5063.
  E-mail address: ms2682@cornell.edu (M.N. Silberstein).
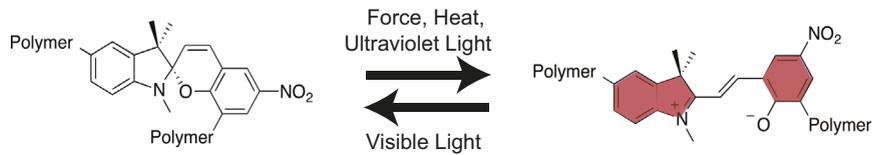
Fig. 1. Ring opening of the spiropyran mechanophore can be induced by force applied at the indicated polymer linkage points, converting the mechanophore to the merocyanine form which has a fluorescent signature. The ring opening can also be induced by exposure to ultraviolet light (~365 nm) or heat and reversed by exposure to visible light (~532 nm).

been extensively investigated. When spiropyran (SP) is linked into a polymer chain, it will transform with applied force to its merocyanine (MC) form via a ring opening reaction (Fig. 1). The state of this mechanophore is optically trackable due to a visible range fluorescence signal present in the MC form, but not detectable in the SP form. Prior results have shown that the mechanically driven conversion rate of SP to MC within PMA is dependent on stretch, orientation, stretch rate, and stretch history (Davis et al., 2009; Beiermann et al., 2011, 2012, in press). The mechanophore can also be driven from SP to MC with exposure to ultraviolet light (UV, ~365 nm) or heat and driven from MC to SP with visible light (~532 nm) (Minkin, 2004).

Here a microstructurally based model is developed to describe the response of mechanophores within solid state bulk elastomers. The model is developed with two broad targets in mind: (1) designing mechanophore-linked polymers to activate under predefined conditions, and (2) using optically trackable mechanophores to better understand force distribution within polymers. PMA is chosen as the host polymer because it is the simplest material for which data exists to benchmark the model. The model integrates results from steered molecular dynamics simulations on the mechanophore together with rubber elasticity theory.

2. Model theory

Mechanophore response within a bulk polymer depends on both the force-dependent rate kinetics of the mechanophore and the rate dependent mechanical behavior of the host polymer. The mechanophore response function and the host polymer response function must be decoupled in order for either of the model targets to be reached. A general model for each of these functions is presented below.

2.1. Mechanophore kinetics

Mechanophore level kinetics are determined using first principles methods that incorporate external force pulling schemes. Ab initio steered molecular dynamics (AISMD) enables predictions of mechanophore reactivity in response to an applied force (Ong et al., 2009). This method employs a constant force scheme whereby applied force is directed to select atomic sites on the mechanophore, consistent with the polymer chain connection points. The AISMD simulations dynamically solve the electronic Schrödinger equation along with the Newtonian dynamics of the atoms, allowing arbitrary rearrangement of covalent bonds. The method has the important attribute of requiring no fitting parameters, but is computationally expensive. AISMD provides information on the reaction mechanism at large forces where the simulations may span from femtosecond to picosecond time scales. To circumvent the cost of running AISMD simulations at experimentally accessible lower forces and longer timescales, a force modified potential energy surface (FMPES) framework is adopted (Ong et al., 2009). The FMPES framework provides knowledge of the minimal energy pathway (MEP) on the potential energy surface, which contains structural information regarding the reactants, transition states, and products. The MEP, which connects the minima to a transition state, can then be optimized for a given external force, providing information on the force perturbed molecular conformations. Additionally, knowledge of the activation barriers as a function of force is obtained along the reaction pathway. Since the MEP along the FMPES provides geometrical information (reactants, transition state), any single bond distance or angle can be monitored along the reaction coordinate. The attempt frequencies for the forward (activation) and reverse (deactivation) reactions can also be determined by using statistical theories, e.g. transition state theory, within the FMPES framework (Fig. 2).

Transition state theory is used to calculate reaction rates that are relevant to laboratory timescales from known force dependent activation barriers and attempt frequencies. A single reactant to single product mechanophore transformation is described by

$$\dot{\alpha} = k_f(1-\alpha) - k_r\alpha, \tag{1}$$

where α is the concentration of mechanophores in the activated (triggered) state, $\dot{x}$ indicates a time rate of change for variable x, k_f is the forward reaction rate, and k_r is the reverse reaction rate. In the case of the mechanophore used here there are two different conformations of the final product. The pathway to each product conformation has its own rate constant:

$$\dot{\alpha}_d = k_{d,f}(1-\alpha) - k_{d,r}\alpha_d, \tag{2}$$

where the subscript d stands for either pathway 1 or pathway 2. The total activated population is the sum of the two conformations:

$$\alpha = \alpha_1 + \alpha_2. \tag{3}$$
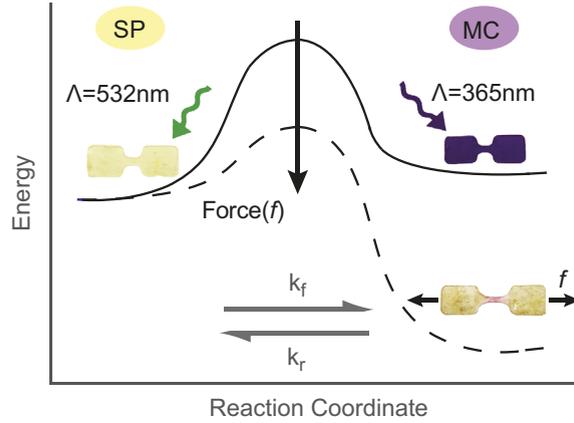
Fig. 2. Schematic of a one-dimensional version of the potential energy surface describing the force accelerated conversion of spiropyran (SP) to merocyanine (MC).

The rate constant is expressed as follows:

$$k_{d,a} = \frac{k_b \theta}{h} \frac{Q_{d,a}^\dagger}{Q_{d,a}} \exp\left[\frac{-\Delta G_{d,a}}{R\theta}\right],$$ (4)

where the subscript a stands for either the forward (f) or reverse (r) reaction, k_b is Boltzmann's constant, θ is the absolute temperature, h is Planck's constant, $Q_{d,a}^\dagger/Q_{d,a}$ is the attempt frequency, $\Delta G_{d,a}$ is the transformation energy barrier, and R is the universal gas constant.

When the external force is sufficiently small, the activation energy depends linearly on the external force (Kauzmann and Eyring, 1940; Bell, 1978), i.e.

$$\Delta G_{d,a} = \Delta G_{d,a}^o + f \Delta x_{d,a},$$ (5)

where f is the applied force and $\Delta x_{d,a}$ is an effective distance between the reactant minimum and transition state geometries. We determine $\Delta x_{d,a}$ from FMPES MEP calculations with two different applied forces and use Eq. (5) to predict activation energies at all forces needed in the mesoscopic simulations. The prefactor $Q_{d,a}^\dagger/Q_{d,a}$ has a secondary influence on reaction kinetics and is also linearly interpolated based on FMPES calculations at the same two applied forces.

2.2. Polymer force distribution

The polymer matrix is responsible for transmitting force from the macroscale to the mechanophores. In the class of materials discussed here, the mechanophore is linked directly in the backbone of a predominantly elastomeric linear polymer. The continuum model is therefore based on rubbery elasticity theory. Each individual polymer chain mechanical response is entropically dominated. The chains interact with each other via an entangled network. Inelasticity is captured by an evolution in the characteristic entanglement spacing.

The total stress response is in general the sum of the elastomeric and glassy responses:

$$\mathbf{T} = \mathbf{T}_N + \mathbf{T}_I,$$ (6)

where $\mathbf{T}$ is the total Cauchy stress, $\mathbf{T}_N$ is the stress due to the elastomeric network, and $\mathbf{T}_I$ is the intermolecular stress associated with the glassy response. Since this model focuses on the interaction of the elastomeric behavior with the mechanophores, details of the glassy mechanical response are left to Appendix B1. The network mechanical model is directly relevant to the activation model and is discussed here in detail.

A strain energy approach is used to determine both the network mechanical response and the polymer chain force. The network Cauchy stress is defined by the derivative of the strain energy density with respect to the deformation gradient:

$$\mathbf{T}_N = \frac{1}{J} \frac{\partial \psi}{\partial \mathbf{F}} \mathbf{F}^\mathsf{T},$$ (7)

where $J = \det \mathbf{F}$ is the volume change, ψ is the network strain energy density, and $\mathbf{F}$ is the deformation gradient. The bulk modulus of the glassy component of the model is used to weakly enforce incompressibility.

Abstracting from Bažant and Oh (1986) and Miehe et al. (2004), the polymer mechanical response is numerically approximated by a discretization into 21 distinct populations of representative chains distributed isotropically about a unit sphere in the reference configuration (Table 1). This approach was selected over the more well known eight-chain or full chains models for its explicit representation of polymer chain force as a function of orientation (see Appendix A). The total

Table 1
21 Chain model approximate orientations and weights.

No.	r_1^i	r_2^i	r_3^i	w^i
1	1.0	0.0	0.0	0.053
2	0.0	1.0	0.0	0.053
3	0.0	0.0	1.0	0.053
4	0.707	0.707	0.0	0.040
5	0.707	0.0	0.707	0.040
6	0.0	0.707	0.707	0.040
7	0.836	0.388	0.388	0.050
8	0.388	0.836	0.388	0.050
9	0.388	0.388	0.836	0.050
10	−0.707	0	0.707	0.040
11	−0.707	0.707	0	0.040
12	0.0	−0.707	0.707	0.040
13	−0.836	0.388	0.388	0.050
14	0.836	−0.388	0.388	0.050
15	−0.836	−0.388	0.388	0.050
16	−0.388	0.836	0.388	0.050
17	0.388	−0.836	0.388	0.050
18	−0.388	−0.836	0.388	0.050
19	−0.388	0.388	0.836	0.050
20	0.388	−0.388	0.836	0.050
21	−0.388	−0.388	0.836	0.050

strain energy density is therefore the weighted average of the strain energy of each of the populations:

$$\psi = \sum_{i=1}^{21} w^i n^i \Psi^i, \tag{8}$$

where w^i is the weighting factor for population i, $w^i n^i$ is the number density of population i, and Ψ^i is the strain energy of population i.

The strain energy of a single polymer chain is entropically based and must account for finite chain extensibility at the forces relevant to mechanophore activation. The strain energy is defined in terms of the stretch on the chain. Following Kuhn (1936) the polymer chain has initial end to end distance $l_o = l_k\sqrt{N}$, where $l_k = l_c/N$ is the Kuhn segment length and N is the number of Kuhn segments along the contour length (l_c) of the polymer chain. The strain energy (Ψ) of a chain is

$$\Psi = k_b \theta N \left(\frac{\lambda}{\sqrt{N}}\beta + \frac{\ln \beta}{\sinh \beta} \right) - \theta c, \tag{9}$$

where $\lambda = l/l_o$ is the chain stretch, β is the inverse Langevin function $\beta = \mathcal{L}^{-1}(\lambda/\sqrt{N})$ for the Langevin function defined as $\mathcal{L}[\beta] = \coth \beta - (1/\beta)$, and c is a constant (Wang and Guth, 1952). The force (f) on the chain is determined from the derivative of the strain energy as

$$f = \frac{1}{l_o}\frac{\partial \Psi}{\partial \lambda} = \frac{k_b \theta}{l_k} \mathcal{L}^{-1}\left(\frac{\lambda}{\sqrt{N}} \right). \tag{10}$$

Within the entangled network framework used here, force is calculated for each population of chains i with N^i Kuhn segments between entanglement points (as opposed to along the entire chain):

$$f^i = \frac{k_b \theta}{l_k} \mathcal{L}^{-1}\left(\frac{\lambda^i}{\sqrt{N^i}} \right) \tag{11}$$

The stretch on each population (λ^i) is kinematically determined by the total deformation gradient assuming affine deformation. (For instance $\lambda^1 = \sqrt{F_{11}^2 + F_{21}^2 + F_{31}^2}$, whereas $\lambda^5 = 0.707\sqrt{(F_{11}+F_{13})^2 + (F_{21}+F_{23})^2 + (F_{31}+F_{33})^2}$). Accounting for inelasticity, the entanglement length evolves separately for each population as

$$\dot{N}^i = \left(\frac{f^i}{f_{ref}} \right)^p \left(1 + \text{sign}\left(\dot{\lambda}^i\right)\left(\frac{|\dot{\lambda}^i|}{\dot{\lambda}_{ref}} \right)^q \right)\left(1 - \frac{N^i}{N} \right), \tag{12}$$

where f_{ref} is a reference force for entanglement slip, $\dot{\lambda}_{ref}$ is a reference stretch rate for entanglement slip, and p and q are constants characterizing the nonlinearity of the force and stretch rate slip dependence respectively. Separate network evolution for each population enables relaxation to be driven locally at the chain populations with the highest force. This network evolution is constrained by

$$n^i N^i = nN \tag{13}$$

where n is the total number density of polymer chains. It is assumed that all chains consist of the same number Kuhn segments and that all chain segments have the same initial number of Kuhn segments between crosslinks. The former assumption is reasonable for materials with a low polydispersity index. The chain specific force driven network slip makes the model fairly insensitive to the latter assumption.

Noting that $\partial \Psi^i / \partial \lambda^i = f^i l_k \sqrt{N^i}$, Eqs. (7) and (8) are combined as

$$\mathbf{T}_N = \frac{1}{J} \left[\sum_{i=1}^{21} w^i n^i f^i l_k \sqrt{N^i} \frac{\partial \lambda^i}{\partial \mathbf{F}} \right] \mathbf{F}^T. \tag{14}$$

It is readily apparent that the network stress is directly a function of the force on each population.

The homogenized activation is given by the activation of each of the populations weighted as for the mechanical response:

$$\langle \alpha \rangle = \sum_{i=1}^{21} w^i \alpha^i, \tag{15}$$

where $\langle \alpha \rangle$ is the homogenized activation (fraction of mechanophores in the activated state) and α^i is the activation state of the ith population.

The activation of each population is calculated according to Section 2.1 where the force in Eq. (5) is now given by the polymer chain population force (Eq. (11)). Results from an additional version of the model will also be presented in which activation is not only influenced by the network stress (T_N), but also the intermolecular stress (T_I). Specifically, the intermolecular stress influence is modeled as an addition to the entropically based chain population force:

$$f_{eff}^i = f^i + \text{sign}(\text{tr } \mathbf{T}_I) \frac{|\mathbf{T}_I'|}{s_f} \tag{16}$$

where $\mathbf{T}_I' = \mathbf{T}_I - \frac{1}{3} \text{tr } \mathbf{T}_I$ is the deviatoric portion of the intermolecular stress and s_f normalizes the stress magnitude to units of force on the atomic scale. Eq. (16) is motivated by the concept that mechanophore activation, like plastic deformation, results from shear loading. For the version of the model including the glassy contribution to activation, f_{eff}^i is substituted for f in Eq. (5).

The theory is implemented in the finite element code Abaqus using an explicit user material subroutine (Vumat). The inverse Langevin function is evaluated using the Padé approximation (Cohen, 1991). Unless otherwise mentioned simulations are performed using a dog-bone geometry and grip conditions corresponding to the benchmark experiments. The strain, stress, and activation are extracted from the center of the gage section across the full width and thickness, in analog to the treatment of the experimental data as will be discussed in Section 3.2. The mechanical properties are determined by a combination of a priori known polymer properties and fits to the stress–strain data. Details are provided in Appendix B.2. The network activation properties are entirely determined by the ab initio FMPES simulations. The intermolecular portion of the activation driving force ($s_f = 9.5$ Pa/nN) is fit to the experimental activation data.

3. Experimental methods

3.1. Materials

Linear mechanochemically active SP-linked PMA was synthesized using SP as a living radical initiator. By this method SP was covalently bonded into roughly the center of the PMA polymer chain. Polymers presented in this study were synthesized with number average molecular weights of 350 kDa, and polydispersity below 1.2. Glass transition temperature (T_g) for the polymer is 12 °C as measured by differential scanning calorimetry.

3.2. Optomechanical characterization

Measurements for load, displacement, and fluorescence intensity were captured simultaneously during tensile testing (Beiermann et al., in press). The SP-linked PMA was hot pressed into dog-bone shaped specimens with gauge length, width, and thickness of 5 mm, 2 mm, and 0.6 mm respectively. The fluorescence response was excited with an 8 mm diameter 532 nm collimated laser. The input laser was shuttered to minimize light-induced reversion of MC to SP. The output fluorescence signal was passed through a long-pass filter for wavelengths greater than 575 nm and collected with a color CCD camera (AVT Stingray F504c). The material was exposed to white light before starting mechanical loading in order to drive the mechanophores to the SP form. Dual actuator stages applied uniaxial tensile loading under displacement control such that both grips moved equal distances in opposite directions, and the sample center was stationary for fluorescence excitation and imaging (Beiermann et al., in press). Two loading histories were applied: (i) "monotonic" loading to failure at a constant grip displacement rate and (ii) "stress relaxation" loading at a constant grip displacement rate to a preset grip displacement followed by a hold at constant grip displacement.

Stretch was calculated locally at the center of the specimen using the optically measured width and assuming isotropy and incompressibility:

$$\lambda_w = \frac{w}{w_o} \tag{17}$$

$$\lambda = \frac{1}{\lambda_w^2} \tag{18}$$

where λ_w is the width stretch ratio, w is the current width, w_o is the initial width, and λ is the stretch. This analysis procedure was necessary due to the large out-of-gauge deformation characteristic of elastomer deformation and the limited field of view. The procedure was validated with a reference sample for which the entire specimen deformation was monitored. True strain was calculated as the natural log of the center region stretch. True stress was calculated as the force divided by the current cross-sectional area.

Three steps were required to convert the raw fluorescence images to an activation value. First the fluorescence was corrected for the change in the number of mechanophores in the region upon which the laser is incident. This correction was taken to be linear with thickness assuming no influence of fluorescence quenching:

$$I_{cor} = \frac{I_{fl,raw}}{\lambda_t} \tag{19}$$

where $\lambda_t = \lambda_w$ is the thickness stretch ratio, $I_{fl,raw}$ is the raw average fluorescence intensity for the material exposed to the laser beam, and I_{cor} is the thickness-corrected fluorescence intensity. Next the fluorescence was converted to a measured activation value assuming minimal initial activation (CCD intensity is non-zero even for specimens with no mechanophores):

$$\alpha_m = \frac{I_{cor} - \min(I_{cor})}{C} \tag{20}$$

where α_m is the measured activation and C is estimated based on the fluorescence intensity of specimens fully activated by UV irradiation and is held the same for all experiments. Finally the activation was corrected to account for the laser deactivation effect since the laser which excites the fluorescence also acts to drive the activated mechanophores (MC) back to the non-fluorescent state (SP) (Fig. 2):

$$\dot{\alpha} = \dot{\alpha}_m - k_{close} \alpha_m \frac{t_{exp}}{t_{frame}} \tag{21}$$

where k_{close} is the rate of laser induced closure calibrated with a load free UV activated specimen exposed to continuous laser light and t_{exp}/t_{frame} is the fraction of time that a specimen is exposed to laser light (controlled by a shutter in front of the specimen). Deactivation due to laser light was negligible under monotonic loading but resulted in a noticeable change in the shape of the activation curve for stress relaxation experiments.

4. Results

4.1. Mechanophore simulations

Minimum energy path calculations on the force modified potential energy surface were performed on the spiropyran (SP) mechanophore at constant forces of 0 and 0.5 nN. The potential energy surface in these calculations is obtained using density functional theory (Hohenberg and Kohn, 1964) with the B3LYP functional (Becke, 1988) and the 6-31G basis set (Becke, 1993). The 0 and 0.5 nN force range is small enough that linear interpolation of the SP-MC energy barrier is a good approximation, but large enough to span most of the forces which are experienced by the mechanophores in the simulation. The activation energies and attempt frequencies associated with each of the two pathways for the forward and reverse reactions are presented in Table 2. The SP to MC energy barriers decrease significantly with applied force whereas the MC to SP energy barriers increase significantly with applied force. The shift in energy barriers results in an increasing percentage of mechanophores in the MC state with an increasing force as expected. There is a noticeable change in attempt frequency

Table 2
Results from ab initio FMPES-MEP simulations of the reversible conversion of SP to MC under constant force.

Force (nN)	$Q_f^\dagger/Q_f$	ΔG_f (J mol^{-1})	$Q_r^\dagger/Q_r$	ΔG_r (J mol^{-1})	Pathway
0	8.59	1.19×10^5	0.839	9.79×10^4	1
0	9.68	1.18×10^5	1.23	1.04×10^5	2
0.5	0.798	5.81×10^4	0.158	1.43×10^5	1
0.5	6.51	5.96×10^4	1.63	1.53×10^5	2

Table 3
Rate constants extracted from ab initio FMPES-MEP simulations of the reversible conversion of SP to MC under constant force. k_f is the sum of the two forward pathways, whereas k_r is estimated as the average of the two reverse pathways.

Force (nN)	k_f (s^{-1})	k_r (s^{-1})
0	1.94×10^{-7}	1.99×10^{-5}
0.5	1.75×10^3	4.84×10^{-14}
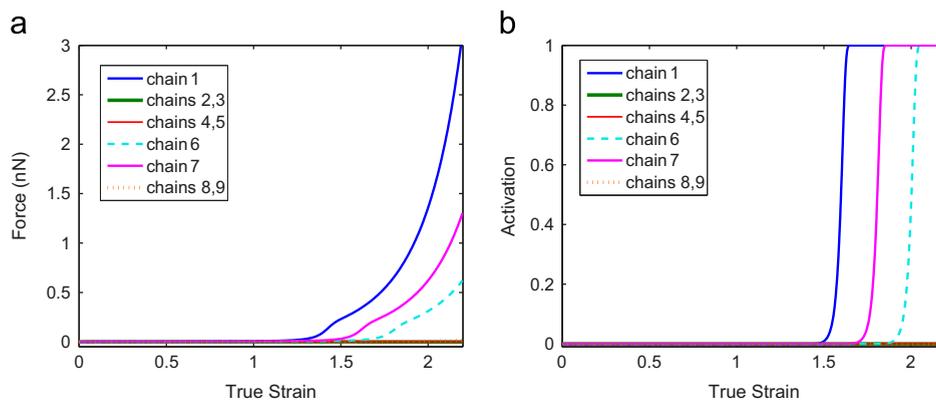
Fig. 3. Behavior of the 21 representative populations under uniaxial stress at a constant engineering strain rate of 0.1 s^{-1}. (a) Force–strain, (b) activation–strain. Note: only the first 9 chains (which fully represent of any principal space deformation) are shown.

with an increasing force for both of the forward and reverse transformations. Given the weak dependence of rate constants on attempt frequency, these changes in attempt frequency have a negligible effect on either the kinetics or equilibrium state.

The rate constants corresponding to the mechanophore results are given in Table 3. A population of mechanophores subjected to a force of 0.5 nN will evolve from the 0 nN equilibrium percentage of 1.5% MC to the 0.5 nN equilibrium concentration of 100% MC within 10 ms, well below the experimental time scale of seconds to hours.

4.2. Continuum simulations and experiments

Each population of chains rotates and stretches affinely with the deformation gradient when pure uniaxial stress is applied. The populations which are most aligned with the primary direction of loading have the most chain stretch and consequently the largest force and earliest activation. Fig. 3 shows the force and activation response of the 9 chains representative of any principal space deformation (the first 9 listed in Table 1) when pure uniaxial stress is applied in the 1-direction. The force response is in the nano-Newton range as is appropriate for mechanophore activation. Chain 1 (perfectly aligned with the 1-direction) has the largest force of all the chains at a given macroscopic strain. The chains which are primarily aligned with the 2nd and 3rd principal directions (2,3,4,5,8,9) do not reach an appreciable force during the loading. The local inelasticity in the model is also evident in Fig. 3a with the force increase of each chain becoming more gradual as the force becomes large enough to activate entanglement slip. Activation of each population follows the force of each population, but is significantly steeper with strain. A steep slope results from the nonlinear force dependence on stretch, coupled with the highly nonlinear activation rate kinetics dependence on force.

The experimental activation response within PMA under monotonic loading is highly rate dependent and largely attributable to the rate dependent stress response of the polymer matrix (Fig. 4). The stress response is predominantly elastomeric. The stress asymptote for the fast rate tests occurs at lower strains than the slow rate tests because there is less time for entanglement slip. The strain rate indicated in the figure corresponds to the engineering strain rate calculated from the crosshead displacement and initial gauge length, however the rate experienced by the region of interest can be significantly less than the nominal rate due to the role of strain hardening in promoting out-of-gauge deformation. The deviation from nominal rate is most extreme for the fastest rate tests which have the most strain hardening and were consistently observed to have slightly non-monotonic strain history prior to failure. A glassy component to the mechanical response is evident in the stress dependence on strain rate at low strain. Activation begins at the lowest strain for the fastest rate of deformation, at the middle strain for the middle rate, and at the largest strain for the slowest rate. For all three rates the activation increases sharply as a function of strain and corresponds closely to network locking in the mechanical response. Fundamentally, the rate dependence of activation is a competition between increasing stress and decreasing time for activation with an increasing strain rate. However, the asymptotic stress response dominates for SP-linked PMA.
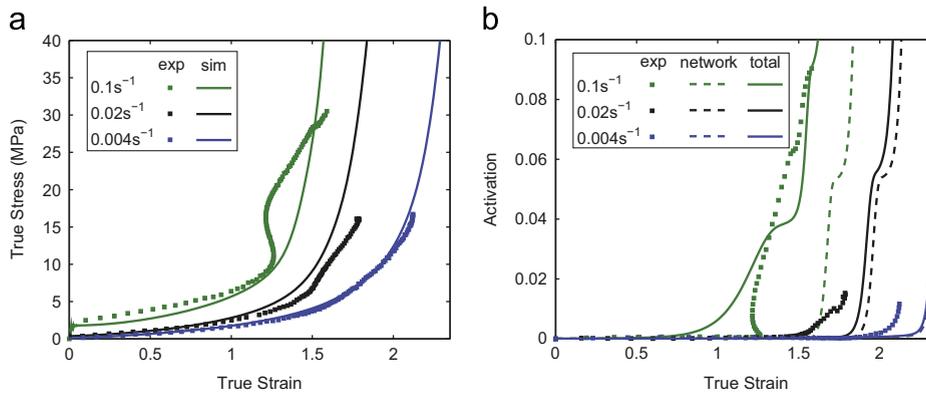
Fig. 4. Experimental and simulated response of SP-linked PMA under monotonic loading at 3 nominal engineering strain rates. (a) Stress–strain, (b) activation–strain. Two sets of activation simulation results are shown: one for the elastomeric network model and one for the total model including the additional glassy driving force.
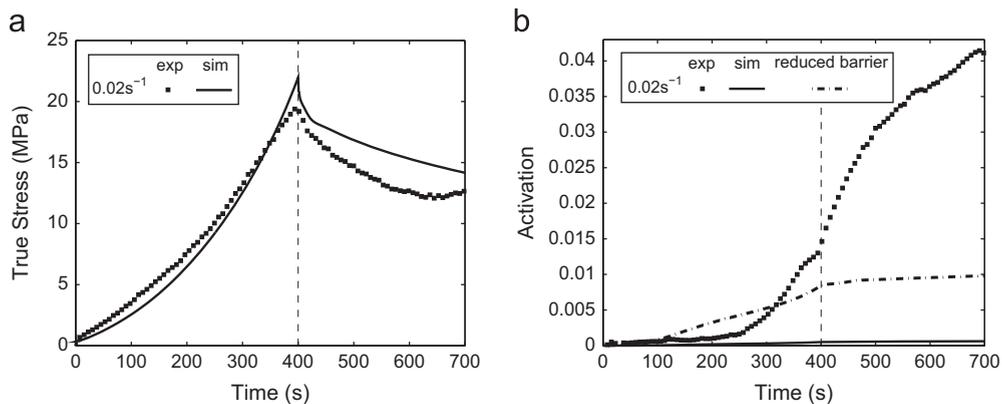
Fig. 5. Experimental and simulated response of SP-linked PMA loaded at a nominal engineering strain rate of 0.02 s^{-1} and then held at constant strain for 300 s. (a) Stress–time, (b) activation–time. The simulation results include the intermolecular driving force. A reduced barrier result is presented for a 7% decrease in the activation energy barriers. The dashed line indicates the beginning of the constant strain portion of the experiment.

The model as described in Section 2.2 is well fit to the monotonic stress–strain response (Fig. 4a). It captures both the glassy rate dependence in the small strain regime and the entangled network rate dependence in the large strain regime. By performing the simulations with the full dog-bone geometry, the experimental strain rate history at the region of interest for each nominal strain rate is reproduced to sufficient accuracy (not shown).

Two versions of the activation model are presented in Fig. 4b. The microstructurally based (network) simulation drives activation directly with the force on each population and provides a reasonable prediction of the activation. Both the shape of the activation–strain response and the rate dependence are similar to the experimental results. The small kinks in the simulated activation–strain response are a result of the 21 discrete chain approximation, showing the discretization to be reasonable. For all three rates, however, the activation becomes measurable at a larger strain than experimentally observed. This strain delay is greatest for the fastest rate test and smallest for the slowest rate test. The rate dependent error motivates the second simulation result shown (total) in which the glassy stress is used as an additional contribution to the activation. The "total" version of the activation model (now with one fitting parameter) more accurately depicts the experimental data at the highest rate, but the shape of the simulated activation is different from the experimentally observed activation indicating that the role of the intermolecular stress is overestimated. At the slowest rate the glassy mechanical response is negligible, yet there is still a difference between the experimental and simulated activation; this difference indicates a need for inclusion of additional factors in the activation response.

When the material is held at a constant strain after monotonic loading, the activation continues to increase at a rate comparable to that during loading, while the stress relaxes to a steady state value (Fig. 5). This activation response is non-intuitive. If the mechanophore responds directly to the macroscopic stress state, the rate of activation is expected to decrease with the stress decay. Continued activation increase with the decreasing stress occurs across different strain rates, hold strains, and even in displacement controlled unloading (not shown).

The activation model compares relatively poorly with the experimental results for stress relaxation loading. As expected from the monotonic simulation results, the model predicts a significantly lower activation at the beginning of the constant

strain portion than seen in the experiment, whereas the stress value is comparable (Fig. 5). In order to compare an activation level more closely matched with the experimental value at the end of the monotonic loading portion, the simulation result for a 7% reduction in both the forward and reverse energy barriers is also shown. The qualitative behavior for this reduced energy barrier simulation is the same as for the standard simulation. During the constant strain regime the simulated stress decrease is similar to the experiment. The simulated activation has some post hold increase, but this slope is smaller than the slope during loading in contrast to the experimentally observed behavior. This qualitative discrepancy is likely related to the quantitative discrepancy in the monotonic response as is discussed in Section 5.

5. Discussion

Inhomogeneity within the elastomer is believed to be the primary cause of the strain-to-activation and time dependence discrepancies between the experiment and model results. While the network model used here allows for variation of force among the polymer chains as a result of orientation, it does not account for inhomogeneity in either the initial entanglement length or force at which entanglement slip can occur and importantly does not include the subsequent time dependent redistribution of that force. Under monotonic loading, force inhomogeneity results in activation at lower strains because the force at some locations is higher than inferred from the macroscopic stress. Under stress relaxation loading, force inhomogeneity results in time delayed activation as regions adjacent to those of high force rotate and stretch to accommodate the high force regions. The data presented in this paper could be used to validate a more sophisticated elastomer model that would capture these inhomogeneity effects more accurately.

The influence of the force free polymer environment on the mechanophore kinetics may also contribute to model deviations from the experiment. Environmental factors can act either to promote the overall rate of reaction (as with a temperature increase) or to shift the equilibrium value (as with a strongly polar environment, Minkin, 2004). Ab initio FMPES simulations have shown that the addition of polymer chain segments to the SP mechanophore connection points has minimal effect on the kinetics (Cremar, 2012), but due to computational limitations surrounding chains have not yet been included. If the polymer environment does significantly influence the mechanophore kinetics then that would be a critical limitation on developing generalized design models in which the polymer matrix and mechanophore can be freely interchanged. The role of the polymer environment requires further investigation either via experiments or AISMD simulations that include surrounding molecules.

6. Conclusions

A continuum framework has been established to describe the activation of force responsive molecules (mechanophores) covalently linked within an elastomer. The theory proposed here ties together transition state theory characterizing the mechanophores with entropically based rubber elasticity that transitions force and activation through the macromolecular to the macroscale. The underlying physical basis of the model is that the polymer chain forces which result in macroscopic stress are the same polymer chain forces that activate the mechanophores. The exponential force dependence of the mechanophore reaction kinetics means that within their active range mechanophores are intrinsically more sensitive than macroscopic stress to polymer chain force.

The model was benchmarked against experimental results for the case of spiropyran linked within the backbone of linear polymethacrylate. SP-linked PMA was chosen because it is a mechanophore–elastomer system for which synthesis and characterization methods have already been established. The elastomer mechanical properties were fit to the PMA tensile stress–strain data. The mechanophore kinetic properties were determined from ab initio minimal energy path calculations on the force-modified potential energy surface at constant force. Activation was then predicted as a function of strain, strain rate, and strain history. The predicted activation showed reasonable agreement with the experimental data, but uniformly underestimated activation for a given strain and underestimated the time dependent increase in activation even as macroscopic stress is reduced. While environmental factors and the glassy component of the stress likely play a role in the apparently altered force dependent kinetics, the observed discrepancies are best understood in terms of local inhomogeneities. As a result of these inhomogeneities, the model functions as a lower bound estimate for activation. While the mechanophore sensitivity to local force is a drawback from the continuum modeling perspective, it could be an asset for studying the local force distribution. Given the nanoNewton scale forces required for SP activation, these mechanophore probes could aid in building an understanding of elastomer deformation and failure processes.

Acknowledgments
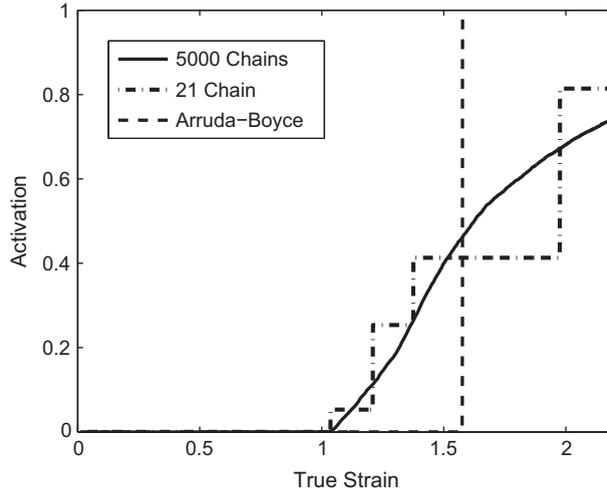
Fig. A1. Activation based on the 21 chain approximation compares favorably to the 5000 chain solution for an ideal elastomer. The Arruda–Boyce based activation result is shown for comparison.

Appendix A. 21 chain model for homogenizing activation response

The 21 chain discretization of the unit sphere was selected to model the mechanical and activation response because it is a reasonable approximation to activation in an incompressible, perfectly affine, perfectly elastic rubbery network. Here, a reference true solution is calculated via a Monte Carlo simulation on 5000 randomly distributed chains, each of which rotate and stretch affinely with the total deformation gradient. A simulation result using the same overall framework but substituting the single representative population from the Arruda–Boyce model (Arruda and Boyce, 1993) for the 21 chains is included for comparison ($\lambda_{AB} = [\sum_{i=1}^{3}(\lambda_i^P)^2/3]^{1/2}$, superscript P indicating principal stretch, subscript i indicating the direction).

Under uniaxial loading the 21 chain model approaches the 5000 chain result in a staircase manner (Fig. A1). This behavior is also seen under biaxial loading (not shown). The discrete behavior exhibited for this highly idealized network is inherently the worst case scenario as any viscous effects in the network will blur the distinction between the forces and activation values of the different initial orientations. The Arruda–Boyce model predicts that activation starts at a much larger strain than the true solution and then becomes complete almost instantaneously. The result using the Arruda–Boyce model highlights the importance of including the orientation distribution.

Appendix B. Mechanical model

B.1. Intermolecular stress

The total Cauchy stress is the sum of the intermolecular and network stresses. The model for the elastic–viscoplastic intermolecular portion is given here.

Kinematics. The total deformation gradient is multiplicatively decomposed into elastic ($\mathbf{F}_I^e$) and plastic ($\mathbf{F}_I^p$) components:

$$\mathbf{F} = \mathbf{F}_I^e \mathbf{F}_I^p \tag{22}$$

Plastic deformation is assumed to be incompressible such that $J_I^p = \det \mathbf{F}_I^p = 1$. For later use, the elastic deformation gradient is decomposed into stretch ($\mathbf{V}_I^e$) and rotation ($\mathbf{R}_I^e$) components:

$$\mathbf{F}_I^e = \mathbf{V}_I^e \mathbf{R}_I^e \tag{23}$$

The rate kinematics are described by the velocity gradient $\mathbf{L} \equiv \dot{\mathbf{F}}\mathbf{F}^{-1}$ which can be decomposed into its elastic ($\mathbf{L}_I^e$) and plastic ($\tilde{\mathbf{L}}_I^p$) components:

$$\mathbf{L} = \mathbf{L}_I^e + \tilde{\mathbf{L}}_I^p \tag{24}$$

$$\mathbf{L}_I^e = \dot{\mathbf{F}}_I^e (\mathbf{F}_I^e)^{-1} \tag{25}$$

$$\tilde{\mathbf{L}}_I^p = \mathbf{F}_I^e \dot{\mathbf{F}}_I^p (\mathbf{F}_I^p)^{-1} (\mathbf{F}_I^e)^{-1} \tag{26}$$

where $\tilde{\mathbf{L}}_I^p$ is the plastic velocity gradient expressed in the loaded configuration. The plastic velocity gradient in the loaded configuration can be taken as the sum of the rate of stretching and the rate of spin.

$$\tilde{\mathbf{L}}_I^p = \tilde{\mathbf{D}}_I^p + \tilde{\mathbf{W}}_I^p \tag{27}$$

where $\tilde{\mathbf{D}}_L^p$ (symmetric tensor) is the rate of plastic stretching and $\tilde{\mathbf{W}}_I^p$ is the rate of plastic spin. Without loss of generality we choose $\tilde{\mathbf{W}}_I^p = 0$. The plastic deformation gradient is then updated by

$$\dot{\mathbf{F}}_I^p = \mathbf{L}_I^p \mathbf{F}_I^p = (\mathbf{F}_I^e)^{-1} \tilde{\mathbf{D}}_I^p \mathbf{F}_I \tag{28}$$

where $\tilde{\mathbf{D}}_I^p$ must be constitutively prescribed.

Constitutive. The material stress state is related to the deformation by the constitutive law for a linear elastic spring:

$$\mathbf{T}_I = \frac{1}{J} \mathcal{L}_I^e [\ln \mathbf{V}_I^e] \tag{29}$$

where $J = \det \mathbf{F}$ is the volume change, $\mathcal{L}_I^e$ is the fourth-order modulus tensor, and $\ln \mathbf{V}_I^e$ is the Hencky strain. It is assumed that the material is initially isotropic and can therefore be defined by any two elastic constants. Here we use the shear modulus μ and the bulk modulus κ:

$$\mathcal{L}_I^e = 2\mu \mathcal{I} + (\kappa - \tfrac{2}{3}\mu) \mathbf{I} \otimes \mathbf{I} \tag{30}$$

where $\mathcal{I}$ and $\mathbf{I}$ are the fourth-order and second-order identity tensors respectively.

The plastic stretching tensor in the loaded configuration is given as the product of the scalar rate of plastic deformation and a direction tensor:

$$\tilde{\mathbf{D}}_I^p = \dot{\gamma}^p \mathbf{N}_I^p \tag{31}$$

where the direction $\mathbf{N}_I^p$ is taken to be coaxial with the deviatoric portion of the intermolecular stress ($\mathbf{T}_I' = \mathbf{T}_I - \tfrac{1}{3}\mathrm{tr}\,\mathbf{T}_I$):

$$\mathbf{N}_I^p = \frac{\mathbf{T}_I'}{|\mathbf{T}_I'|} \tag{32}$$

The scalar rate of plastic deformation is constitutively prescribed to follow a rate dependent process driven by the shear stress:

$$\dot{\gamma}^p = \dot{\gamma}^o \exp\left[\frac{-\Delta G}{k_b \theta}\right] \sinh\left[\frac{\Delta G}{k_b \theta} \frac{\tau}{s + c_h(\lambda_{ch} - 1)}\right] \tag{33}$$

where $\tau = \sqrt{\tfrac{1}{2}\mathbf{T}_I' \mathbf{T}_I'}$ is the scalar equivalent shear stress, $\dot{\gamma}_o$ is a pre-exponential factor proportional to the attempt frequency, ΔG is the shear yield activation energy, s is the isotropic shear resistance, c_h is the isotropic hardening slope, $\lambda_{ch} = [\mathrm{tr}(\mathbf{F}\mathbf{F}^{\mathrm{T}})/3]^{1/2}$ is a scalar description of the material deformation, k_b is Boltzmann's constant, and θ is the absolute temperature.

B.2. Material parameters

Network mechanical. The network stress is given by

$$\mathbf{T}_N = \frac{1}{J}\left[\sum_{i=1}^{21} w^i n^i f^i l_k \sqrt{N^i} \frac{\partial \lambda^i}{\partial \mathbf{F}}\right] \mathbf{F}^{\mathrm{T}} \tag{34}$$

$$f^i = \frac{k_b \theta}{l_k} \mathcal{L}^{-1}\left(\frac{\lambda^i}{\sqrt{N^i}}\right) \tag{35}$$

The Kuhn segment length as well as the time dependent number density of effective chains and number of Kuhn segments between cross-links is required to describe the mechanical response.

The total number of chains per unit volume (n) is given by the polymer density and chain molecular weight as

$$n = \frac{\rho}{M_w} \tag{36}$$

The molecular weight of the polymer can also be used to determine the total number of monomers per chain. The total fully entropically extended length of each chain (l_c) is given by the length of each monomer unit ($l_{unit} = 0.25$ nm) based on equilibrium bond lengths and angles and the number of monomers:

$$l_c = l_{unit} \frac{M_w}{M_{unit}} \tag{37}$$

where M_{unit} is the molecular weight of each monomer and M_w/M_{unit} is the number of monomers.

The observed mechanical response is used to determine the remainder of the material parameters. Physically, the number of segments between cross-links sets the locking stretch. The initial number of segments between cross-links (N^o) is set according to the fastest rate experiment since this has the least entanglement slip. The product of the initial effective chain density and the Kuhn segment length ($n^o l_k$) determines the initial rubbery modulus. The slowest rate data is used to identify the initial rubbery modulus since there is minimal contribution from the material glassy behavior. Since these two

parameters cannot be determined from a single observed property, an additional relation is required. We employ what is essentially conservation of mass, requiring that the total initial contour length of effective chains is the same as the total length of actual chains:

$$l_k n N = l_k n^o N^o \tag{38}$$

This assertion introduces an additional unknown N, the number of Kuhn segments in a full chain. N is directly related to the total contour length and the Kuhn segment length:

$$N = \frac{l_c}{l_k} \tag{39}$$

N, n^o, and l_k are thereby simultaneously fit according to the known values of the rubbery modulus, the total chain contour length, the total number of chains when no entanglements are present, and the initial number of Kuhn segments between cross-links.

As entanglement slip occurs the number density of effective chain segments decreases toward the number density of actual full chains and the number of Kuhn segments between cross-links increases toward the total number of segments in a full chain. This evolution is described by

$$\dot{N}^i = \left(\frac{f^i}{f_{ref}}\right)^p \left(1 + \text{sign}\left(\dot{\lambda}^i\right)\left(\frac{|\dot{\lambda}^i|}{\dot{\lambda}_{ref}}\right)^q\right)\left(1 - \frac{N^i}{N}\right) \tag{40}$$

$\dot{\lambda}_{ref}$ is arbitrarily set just below the range of conducted experiments. p, q, and f_{ref} are simultaneously fit to the locking stretch and locking slope for the stress–strain response of the 3 rates at which the experiments were conducted.

Intermolecular mechanical. The intermolecular material parameters are fit from the stress–strain response below a strain of 0.2. The required elastic parameters are the shear (μ) and bulk (κ) modulus. These are fit to the initial slope of the fast rate data ($E = 196$ MPa) with an assumed Poisson's ratio of $\nu = 0.4$, since the initial network modulus is negligible relative to the initial glassy modulus:

$$\mu = \frac{E}{2(1+\nu)} \tag{41}$$

$$\kappa = \frac{E}{3(1-2\nu)} \tag{42}$$

$\dot{\gamma}^o$, ΔG, and s define the rate and temperature dependent initial yield point. Since experiments were only conducted at one temperature only two of these parameters can be uniquely defined. ΔG is therefore set to a typical but arbitrary value. $\dot{\gamma}^o$ and s are then fit to the intercept and slope of the log rate versus yield stress relationship for the three rates of testing. Post-yield intermolecular hardening is relatively minor compared to network hardening and is accounted for by c_h. It is set to the difference between the network based hardening and the fastest rate experimentally observed hardening.

The mechanical material parameters are listed in Table A1.

Table A1
Material parameters for 21 chain mechanical model.

Model component	Material parameter	Value
	n	1.7×10^{24} m^{-3}
	l_c	1.02×10^{-6} m
Network		
Elastic	N^o	8.0
	N	350
Viscoplastic	f_{ref}	1.1×10^{-5} N
	$\dot{\lambda}_{ref}$	1.0×10^{-3} s^{-1}
	p	0.35
	q	0.8
Intermolecular		
Elastic	μ	70 MPa
	κ	330 MPa
Plastic	$\dot{\gamma}^o$	5.0×10^{10} s^{-1}
	ΔG	7.0×10^{-20} J
	s	0.72 MPa
	c_h	4.0 MPa

References

Arruda, E.M., Boyce, M.C., 1993. A three-dimensional constitutive model for the large stretch behavior of rubber elastic materials. J. Mech. Phys. Solids 41, 389–412.

Bažǎnt, Z.P., Oh, B.H., 1986. Efficient numerical integration on the surface of a sphere. Z. Angew. Math. Mech. 66, 37–49.

Becke, A.D., 1988. Density-functional exchange energy approximation with correct asymptotic-behavior. Phys. Rev. A 38, 3098–3100.

Becke, A.D., 1993. Density-functional thermochemistry 3. The role of exact exchange. J. Chem. Phys. 7, 5648–5652.

Beiermann, B.A., Kramer, S.L.B., May, P.A., Moore, J.S., White, S.R., Sottos, N.R., 2012. Role of mechanophore orientation in mechanochemical reactions. ACS Macro Lett. 1, 163–166.

Beiermann, B.A., Davis, D.A., Kramer, S.L.B., May, P.A., Moore, J.S., Sottos, N.R., White, S.R., 2011. Environmental effects on mechanochemical activation of spiropyran in linear PMMA. J. Mater. Chem. 21, 8443–8447.

Beiermann, B.A., Kramer, S.L.B., May, P.A., Moore, J.S., White, S.R., Sottos, N.R. Combined mechanical, birefringence, and fluorescence studies of force-induced chemical reactions in an elastomeric polymer Adv Funct Mater, http://dx.doi.org/10.1002/adfm.20130234, in press.

Bell, G.I., 1978. Models for specific adhesion of cells to cells. Science 200, 618–627.

Black, A.L., Orlicki, J.A., Craig, S.L., 2011. Mechanochemically triggered bond formation in solid-state polymers. J. Mater. Chem. 21, 8460–8465.

Caruso, M.M., Davis, D.A., Shen, Q., Odom, S.A., Sottos, N.R., White, S.R., Moore, J.S., 2009. Mechanically-induced chemical changes in polymeric materials. Chem. Rev. 109, 5755–5798.

Cohen, A., 1991. A Padé approximate to the inverse Langevin function. Rheol. Acta 30, 270–273.

Cremar, L.D., 2012. Insights for Designing Mechanochromic Spiropyrans from First Principles Dynamics and Minimum Energy Pathways (Ph.D. thesis). Stanford University, Palo Alto, CA.

Davis, D.A., Hamilton, A., Yang, J., Cramer, L.D., Gough, D.V., Potisek, S.L., Ong, M.T., Braun, P.V., Martinez, T.J., White, S.R., Moore, J.S., Sottos, N.S., 2009. Force-induced activation of covalent bonds in mechanoresponsive polymeric materials. Nat. Lett. 459, 68–72.

Hickenboth, C.R., Moore, J.S., White, S.R., Sottos, N.R., Baudry, J., Wilson, S.R., 2007. Biasing reaction pathways with mechanical force. Nature 446, 423–427.

Hohenberg, P., Kohn, W., 1964. Inhomogeneous electron gas. Phys. Rev. B 136, B864–B871.

Kauzmann, W.J., Eyring, H., 1940. The viscous flow of large molecules. J. Am. Chem. Soc. 62, 3113–3125.

Kingsbury, C.M., May, P.A., Davis, D.A., White, S.R., Moore, J.S., Sottos, N.R., 2011. Shear activation of mechophore-crosslinked polymers. J. Mater. Chem. 21, 8381–8388.

Kuhn, W., 1936. Relationship between molecular size, static molecular shape and elastic characteristics of high polymer materials. Kolloid-Zeitschrift 76, 258–271.

Lee, C.K., Davis, D.A., White, S.R., Moore, J.S., Sottos, N.R., Braun, P.V., 2010. Force-induced redistribution of chemical equilibrium. J. Am. Chem. Soc. 132, 16107–16111.

Miehe, C., Göktepe, S., Lulei, F., 2004. A micro-macro approach to rubber-like materials-Part I: the non-affine micro-sphere model of rubber elasticity. J. Mech. Phys. Solids 52, 2617–2660.

Minkin, V.I., 2004. Photo-, thermo-, solvato-, and electrochromic spiroheterocyclic compounds. Chem. Rev. 104, 2751–2776.

Ong, M.T., Leiding, J., Hongli, T., Virshup, A.M., Martinez, T.J., 2009. First principles dynamics and minimum energy pathways for mechanochemical ring opening of cyclobutene. J. Am. Chem. Soc. Commun. 131, 6377–6379.

Wang, M.C., Guth, E., 1952. Statistical theory of networks of non-gaussian flexible chains. J. Chem. Phys. 20, 1144–1157.